

Investigation of Hydridosilsesquioxane-Based Silicon Oxide Deposition on Si(111)-7 × 7

Kevin S. Schneider,[†] Thomas M. Owens,[†] Kenneth T. Nicholson,[†]
Bonnie J. Ludwig,[†] J. Neil Greeley,[†] Bradford G. Orr,^{*,‡,§} and
Mark M. Banaszak Holl^{*,†,§}

Chemistry Department, University of Michigan, Ann Arbor, Michigan 48109-1055,
and Physics Department and the Applied Physics Program, University of Michigan,
Ann Arbor, Michigan 48109-1120

Received February 8, 2002. In Final Form: May 28, 2002

X-ray photoemission spectroscopy (XPS), low-energy electron diffraction (LEED), reflection–absorption infrared spectroscopy (RAIRS), and scanning tunneling microscopy (STM) have been used to characterize the discontinuous oxide films formed following exposure of gaseous H₈Si₈O₁₂ hydridosilsesquioxane clusters to Si(111)-7 × 7. Collectively, the four surface characterization techniques support a reaction involving cluster decomposition on the Si(111)-7 × 7 surface. The decomposition of H₈Si₈O₁₂ upon reaction with Si(111)-7 × 7 is in stark contrast with that of the reaction of H₈Si₈O₁₂ with Si(100)-2 × 1 in which the cluster cage remains intact.

Introduction

The oxidation of silicon is one of the most important processes in the microelectronics industry;¹ however, a detailed understanding of the oxidation process and the structure of the resultant Si/SiO₂ interface remains elusive. The demand for smaller, faster metal–oxide–semiconductor (MOS) device components necessitates the creation of thinner, stable insulating oxide layers. For decades, numerous experimental^{2–32} and theoretical^{33–38}

techniques have been employed to gain a better understanding of the oxidation process. Despite this wealth of information, the characterization of the oxidation process and structure of ultrathin oxide films remains controversial and poorly understood.^{9,17,39–41} In principle, the use of well-defined precursor molecules allows control of the structure of the resulting oxide film and provides self-limiting deposition conditions. Such studies can also provide benchmark chemical and spectroscopic data for thin silicon oxide films and the Si/SiO₂ interfacial region.^{42–49}

* Corresponding authors. E-mail: mbanasza@umich.edu, orr@umich.edu.

[†] Chemistry Department.

[‡] Physics Department.

[§] Applied Physics Program.

(1) Massoud, H. Z.; Poindexter, E. H.; Helms, C. R. *The Physics and Chemistry of SiO₂ and the Si-SiO₂ Interface*—3; The Electrochemical Society: Pennington, NJ, 1996.

(2) Ibach, H.; Bruchmann, H. D.; Wagner, H. *Appl. Phys. A* **1982**, *29*, 113.

(3) Hollinger, G.; Himpfel, F. J. *Phys. Rev. B* **1983**, *28*, 3651.

(4) Höfer, U.; Morgen, P.; Wurth, W.; Umbach, E. *Phys. Rev. Lett.* **1985**, *55*, 2979.

(5) Schell-Sorokin, A. J.; Demuth, J. E. *Surf. Sci.* **1985**, *157*, 273.

(6) Hollinger, G.; Morar, J. F.; Himpfel, F. J.; Hughes, G.; Jordan, J. L. *Surf. Sci.* **1986**, *168*, 609.

(7) D'Evelyn, M. P.; Nelson, M. M.; Engel, T. *J. Vac. Sci. Technol., A* **1987**, *5*, 642.

(8) Koch, R. H.; Hamers, R. J. *Surf. Sci.* **1987**, *181*, 333.

(9) Himpfel, F. J.; McFeely, F. R.; Taleb-Ibrahimi, A.; Yarmoff, J. A.; Hollinger, G. *Phys. Rev. B* **1988**, *38*, 6084.

(10) Hamers, R. J.; Koch, R. H. In *The Physics and Chemistry of SiO₂ and the Si-SiO₂ Interface*; Helms, C. R., Deal, B. E., Eds.; Plenum: New York, 1988; p 201.

(11) Leibsle, F. M.; Samsavar, A.; Chiang, T.-C. *Phys. Rev. B* **1988**, *38*, 5780.

(12) Engstrom, J. R.; Nelson, M. M.; Engel, T. *J. Vac. Sci. Technol., A* **1989**, *7*, 1837.

(13) Höfer, U.; Pushmann, A.; Coulman, D.; Umbach, E. *Surf. Sci.* **1989**, *211*, 948.

(14) Morgen, P.; Hofer, U.; Wurth, W.; Umbach, E. *Phys. Rev. B* **1989**, *39*, 3720.

(15) Gupta, P.; Mak, C. H.; Coon, P. A.; George, S. M. *Phys. Rev. B* **1989**, *40*, 7739.

(16) Höfer, U.; Morgen, P.; Wurth, W.; Umbach, E. *Phys. Rev. B* **1989**, *40*, 1130.

(17) Himpfel, F. J.; Meyerson, B. S.; McFeely, F. R.; Morar, J. F.; Taleb-Ibrahimi, A.; Yarmoff, J. A. *Core Level Spectroscopy at Silicon Surfaces and Interfaces*; Campagna, M., Rosei, R., Eds.; North Holland: New York, 1990; p 203.

(18) Engstrom, J. R.; Engel, T. *Phys. Rev. B* **1990**, *41*, 1038.

(19) Pelz, J. P.; Koch, R. H. *Phys. Rev. B* **1990**, *42*, 3761.

(20) Lyo, I.-W.; Avouris, P.; Schubert, B.; Hoffmann, R. *J. Phys. Chem.* **1990**, *94*, 4400.

(21) Tokumoto, H.; Miki, K.; Murakami, H.; Bando, H.; Ono, M.; Kajimura, K. *J. Vac. Sci. Technol., A* **1990**, *8*, 255.

(22) Engstrom, J. R.; Bonser, D. J.; Nelson, M. M.; Engel, T. *Surf. Sci.* **1991**, *256*, 317.

(23) Sakurai, T.; Hasegawa, Y.; Hashizume, T.; Kamiya, I.; Ide, T.; Sumita, I.; Pickering, H. W.; Hyodo, S. *J. Vac. Sci. Technol., A* **1990**, *8*, 259.

(24) Avouris, P.; Lyo, I.-W. *Surf. Sci.* **1991**, *242*, 1.

(25) Avouris, P.; Lyo, I.-W.; Bozso, F. *J. Vac. Sci. Technol., B* **1991**, *9*, 424.

(26) Pelz, J. P.; Koch, R. H. *J. Vac. Sci. Technol., B* **1991**, *9*, 775.

(27) Bozso, F.; Avouris, P. *Phys. Rev. B* **1991**, *44*, 9129.

(28) Mortensen, K.; Chen, D. M.; Bedrossian, P. J.; Golovchenko, J. A.; Besenbacher, F. *Phys. Rev. B* **1991**, *43*, 1816.

(29) Engstrom, J. R.; Bonser, D. J.; Engel, T. *Surf. Sci.* **1992**, *268*, 238.

(30) Seiple, J.; Pecquet, J.; Meng, Z.; Pelz, J. P. *J. Vac. Sci. Technol., A* **1993**, *11*, 1649.

(31) Engel, T. *Surf. Sci. Rep.* **1993**, *18*, 91.

(32) Hamers, R. J.; Wang, Y. *Chem. Rev.* **1996**, *96*, 1261.

(33) Goddard, W. A.; Redondo, A.; McGill, T. C. *Solid State Commun.* **1976**, *18*, 981.

(34) Chen, M.; Batra, I. P.; Brundle, C. R. *J. Vac. Sci. Technol.* **1979**, *16*, 1216.

(35) Ciraci, S.; Ellialtioglu, S.; Erkoç, S. *Phys. Rev. B* **1982**, *26*, 5716.

(36) Batra, I. P.; Bagus, P. S.; Hermann, K. *Phys. Rev. Lett.* **1984**, *52*, 384.

(37) Schubert, B.; Avouris, P.; Hoffmann, R. *J. Chem. Phys.* **1993**, *98*, 7593.

(38) Schubert, B.; Avouris, P.; Hoffmann, R. *J. Chem. Phys.* **1993**, *98*, 7606.

(39) Grunthaner, F. J.; Grunthaner, P. J. *Mater. Sci. Rep.* **1986**, *1*, 65.

(40) Hattori, T. *Crit. Rev. Solid State Mater. Sci.* **1995**, *20*, 339.

(41) Iwata, S.; Ishizaka, A. *J. Appl. Phys.* **1996**, *79*, 6653.

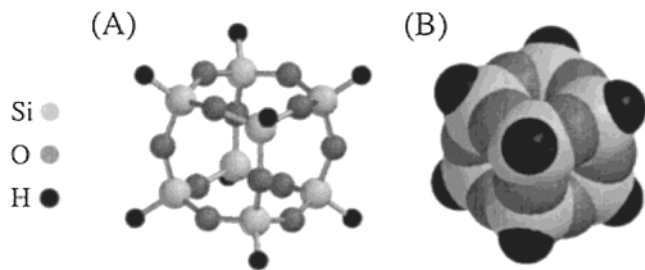


Figure 1. $\text{H}_8\text{Si}_8\text{O}_{12}$. (A) Ball and stick model. (B) Space-filling model. Silicon, oxygen, and hydrogen atoms occupy cluster corners, edges, and corner vertices, respectively.

Hydridosilsesquioxane clusters $[(\text{HSiO}_{1.5})_n; n = 8, 10, 12, 14]^{50,51}$ are volatile, well-defined cage molecules known to chemically react with $\text{Si}(100)\text{-}2 \times 1$, resulting in the formation of a stable, chemisorbed layer of closely packed clusters.⁴² Conventional and synchrotron X-ray photoemission spectroscopy (XPS),^{42,43,46} reflection-absorption infrared spectroscopy (RAIRS),^{47,48,52,53} low-energy electron diffraction (LEED),⁴⁸ and scanning tunneling microscopy (STM)⁴⁹ have been employed to characterize the bonding configuration of $\text{H}_8\text{Si}_8\text{O}_{12}$ chemisorbed to $\text{Si}(100)\text{-}2 \times 1$. All four experimental techniques support a bonding geometry in which a single vertex of the intact cluster cage is bound to a surface silicon dimer atom. Perhaps most convincingly, internal resolution of the electronic states of an individual chemisorbed $\text{H}_8\text{Si}_8\text{O}_{12}$ cluster achieved by STM supports attachment to $\text{Si}(100)\text{-}2 \times 1$ via a single vertex.⁴⁹

$\text{H}_8\text{Si}_8\text{O}_{12}$ (Figure 1) has previously been shown to chemically react with the $\text{Si}(111)\text{-}7 \times 7$ surface, albeit in a decreased quantity relative to $\text{Si}(100)\text{-}2 \times 1$.⁴³ Core-level Si 2p XPS data indicate the presence of a small cluster-derived peak at ~ 3.8 eV (shifted relative to bulk Si), attributed to HSiO_3 units derived from $\text{H}_8\text{Si}_8\text{O}_{12}$. Additionally, a larger Si^+ peak at ~ 1.0 eV is evident as a pronounced shoulder on the bulk Si peak. This feature has been primarily attributed to the presence of other contaminants (H_2O) in the system. Despite this previous characterization, little experimental information has been garnered that offers a detailed explanation of the reaction of $\text{H}_8\text{Si}_8\text{O}_{12}$ with $\text{Si}(111)\text{-}7 \times 7$ and the subsequent structures formed. In this paper, we report new XPS, LEED, RAIRS, and STM data for the reaction of $\text{H}_8\text{Si}_8\text{O}_{12}$ with the $\text{Si}(111)\text{-}7 \times 7$ surface. These data collectively support a reaction pathway involving cluster decomposi-

tion upon reaction of $\text{H}_8\text{Si}_8\text{O}_{12}$ with the surface. Interestingly, the reaction of $\text{H}_8\text{Si}_8\text{O}_{12}$ on $\text{Si}(111)\text{-}7 \times 7$ is profoundly different than that on $\text{Si}(100)\text{-}2 \times 1$, in which the cluster cage remains intact. These observations highlight the importance of the specific reaction pathway for the fate of incoming adsorbates on silicon surfaces.

Experimental Section

Octahydridosilsesquioxane, $\text{H}_8\text{Si}_8\text{O}_{12}$, was synthesized by the method of Agaskar and sublimed twice.^{50,51} Cluster purity was checked using ^1H NMR, IR, and gas chromatography-mass spectrometry. After loading the clusters into a glass or stainless steel ultrahigh vacuum (UHV) compatible sample container, the samples were further purified by sublimation via gentle heating in a water bath at ~ 323 K and prolonged exposure to pumping (> 24 h) in UHV conditions. Clean $\text{Si}(111)$ and/or $\text{Si}(100)$ samples were exposed to 10 to > 1000 L ($\text{L} = \text{Langmuir} = 1 \times 10^{-6}$ Torr-s) of gaseous $\text{H}_8\text{Si}_8\text{O}_{12}$ at typical dosing pressures of 4×10^{-8} to 4×10^{-7} Torr.

Because silicon is highly transparent in the IR spectral region of interest, reflective buried-metal-layer $\text{Si}(111)$ and $\text{Si}(100)$ samples were used for RAIRS experiments.^{54,55} Sample preparation procedures for RAIRS, LEED, and XPS experiments have been explained elsewhere.^{48,52}

Soft-XPS experiments were performed at beamline U8B at the National Synchrotron Light Source (NSLS) at Brookhaven National Laboratory. An incident photon energy of 170 eV was used for the collection of Si 2p core-level and valence band spectra. The spectrometer and beamline have been previously described.^{9,56} Conventional XPS experiments were performed using a PHI5000C spectrometer; the details of which are explained elsewhere.⁴³ LEED images were obtained with an electron gun energy of 68 eV at ~ 2 nA beam current. The RAIRS (Bio-Rad FTS-40 FTIR spectrometer) and LEED (VG Microtech Rear View spectrometer) experimental apparatus have also been previously described.⁴⁸ Curve fitting was performed with Matlab v4.2c and either PHI-MAT v 4.0 or ESCA Tools v.4.2. Standard methods were employed for the deconvolution of the Si 2p spin-orbit doublet in XPS core-level spectra.^{9,56}

Small (~ 3 mm \times 7 mm \times 0.25 mm) $\text{Si}(111)$ samples for STM imaging experiments were cut from a larger wafer (Virginia Semiconductor, n-type, As-doped, resistivity $\sim 0.001 \Omega\text{-cm}$) and rinsed with acetone and methanol before being loaded into the UHV chamber. Samples were degassed at 873–973 K by resistive heating in UHV for at least 12 h (temperatures measured with a Minolta-Land infrared optical pyrometer; Cyclops 52, emissivity setting 0.7). Desorption of native oxide layers on degassed samples was accomplished by flashing to ~ 1350 K for 30 s followed by annealing at ~ 923 K for 30 s, yielding the (7×7) reconstruction with a low defect density. Prior to dosing with clusters, sample structure was assessed by STM.

STM images were acquired at room temperature in the constant-current mode using an RHK Technology, Inc., UHV300 Series variable-temperature STM at typical sample biases (V_s) of -1 to -2 V and tunneling currents (I_T) of $0.5\text{--}2$ nA. Commercially fabricated platinum/iridium (80/20) STM tips (Materials Analytical Services "Controlled Geometry" Pt/Ir STM tips) were used for imaging. Tip cleaning was accomplished by holding the tip directly above a $\text{Si}(111)$ sample (outside of tunneling range) heated to ~ 1023 K for 10–20 min prior to imaging. Image processing of STM constant-current topographs consisted of plane and slope subtractions; image filters were not employed. Matlab v4.2c was utilized for curve fitting the STM height histogram data (peak height, position, and width were allowed to vary).

(54) The buried-metal-layer $\text{Si}(111)$ and $\text{Si}(100)$ samples were purchased from S. Mantl, Institute für Schicht- und Ionentechnik, Forschungszentrum Jülich GmbH, P. O. Box 1913, 5170 Jülich, Germany.

(55) Ehrley, W.; Butz, R.; Mantl, S. *Surf. Sci.* **1991**, *248*, 193.

(56) Himpfel, F. J.; McFeely, F. R.; Morar, J. F.; Taleb-Ibrahimi, A.; Yarnoff, J. A. *Proceedings of the 1988 Enrico Fermi School on Photoemission and Absorption Spectroscopy of Solids and Interfaces with Synchrotron Radiation*; North Holland: Varenna, 1988.

(42) Banaszak Holl, M. M.; McFeely, F. R. *Phys. Rev. Lett.* **1993**, *71*, 2441.

(43) Lee, S.; Mekan, S.; Banaszak Holl, M. M.; McFeely, F. R. *J. Am. Chem. Soc.* **1994**, *116*, 11819.

(44) Banaszak Holl, M. M.; Lee, S.; McFeely, F. R. *Appl. Phys. Lett.* **1994**, *65*, 1097.

(45) Zhang, K. Z.; Banaszak Holl, M. M.; Bender IV, J. E.; Lee, S.; McFeely, F. R. *Phys. Rev. B* **1996**, *54*, 7686.

(46) Zhang, K. Z.; Meeuwenberg, L. M.; Banaszak Holl, M. M.; McFeely, F. R. *Jpn. J. Appl. Phys.* **1997**, *36*, 1622.

(47) Greeley, J. N.; Banaszak Holl, M. M. *Inorg. Chem.* **1998**, *37*, 6014.

(48) Greeley, J. N.; Meeuwenberg, L. M.; Banaszak Holl, M. M. *J. Am. Chem. Soc.* **1998**, *120*, 7776.

(49) Schneider, K. S.; Zhang, Z.; Banaszak Holl, M. M.; Orr, B. G.; Pernisz, U. C. *Phys. Rev. Lett.* **2000**, *85*, 602.

(50) Agaskar, P. A. *Inorg. Chem.* **1991**, *30*, 2707.

(51) Agaskar, P. A.; Klempere, W. G. *Inorg. Chim. Acta* **1995**, *229*, 355.

(52) Eng, J. J.; Raghavachari, K.; Struck, L. M.; Chabal, Y. J.; Bent, B. E.; Banaszak Holl, M. M.; McFeely, F. R.; Michaels, A. M.; Flynn, G. W.; Christman, S. B.; Chaban, E. E.; Williams, G. P.; Radermacher, K.; Mantl, S. *J. Chem. Phys.* **1998**, *108*, 8680.

(53) Nicholson, K. T.; Banaszak Holl, M. M. *Phys. Rev. B* **2001**, *64*, 155317.

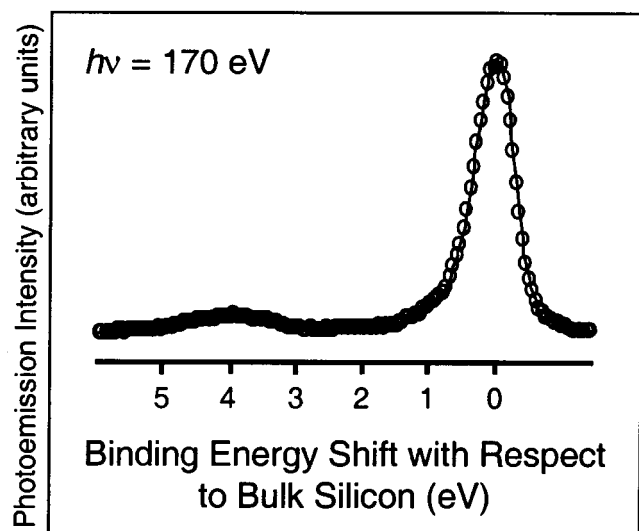


Figure 2. Si $2p_{3/2}$ core level spectrum of the Si(111)-7 × 7 surface following exposure to >1000 L of $H_8Si_8O_{12}$. The Si $2p_{1/2}$ component has been mathematically removed.

Results and Discussion

This section presents the results of XPS, LEED, RAIRS, and STM experiments examining the nature of the reactivity of $H_8Si_8O_{12}$ clusters with Si(111)-7 × 7. Throughout, the data obtained are used to derive estimates of the amount of oxide formation on the surface. It is imperative that one realizes the experimental techniques employed measure fundamentally different surface characteristics. Si 2p and O 1s core-level photoemission spectroscopy measures the kinetic energies of photoelectrons emitted from surface Si and O atoms, respectively. The information garnered from XPS can be used to calculate specific atom concentrations on the sample surface. LEED measures the degree of long-range surface order and can detect changes in the symmetry of the surface. However, it cannot directly ascribe changes observed to physical or chemical effects. RAIRS detects oscillating dipoles of varying strengths. Dipole moments arise as a result of the interaction of a pair or group of atoms, differentiating quantitative analysis of oxide formation as measured by infrared from that derived from photoemission data. Lastly, STM images are limited by the tunneling probabilities of surface features at or near the sample Fermi energy over an extended atomic lattice. Consequently, quantitative interpretation of STM data is distinguished from XPS and RAIRS data that are derived from spectroscopically detectable characteristics of individual and relatively small groups of atoms, respectively. Thus, apparent “surface coverage” values, whether experimentally calculated or inferred, are representative of the unique surface characteristics measured by each experimental technique. These effects give rise to measured values of the amount of oxide on the Si surface that vary by a considerable amount. This variance, when considered in concert with the physical basis of the measurement, allows one to assess both the amount of oxide present on the surface and the nature of its distribution.

I. XPS Data. Exposing a clean Si(111)-7 × 7 surface to >1000 L of gaseous $H_8Si_8O_{12}$ results in a small amount of cluster-derived signal, as shown in the Si $2p_{3/2}$ core-level spectrum displayed in Figure 2, indicating a small number of clusters adsorb to the surface. A small peak appears at ~3.8 eV (shifted relative to bulk silicon), in good agreement with the originally published spectrum and consistent with $HSiO_3$ units derived from $H_8Si_8O_{12}$;

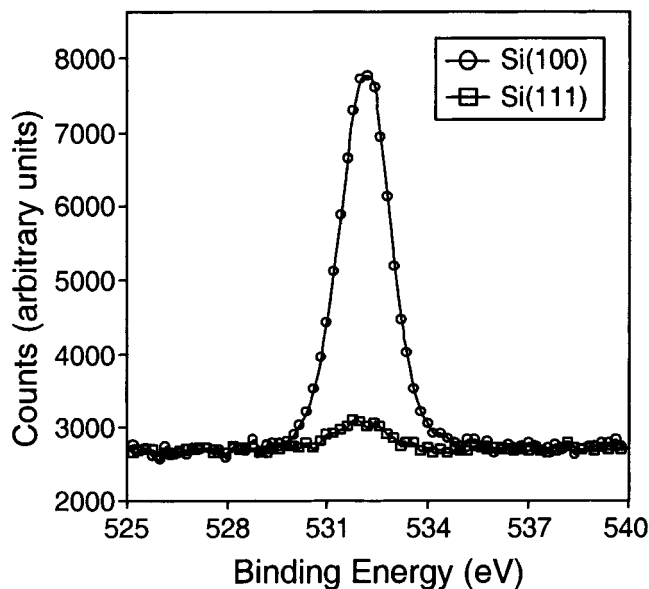


Figure 3. O 1s core-level photoemission data of Si(100)-2 × 1 (circles) and Si(111)-7 × 7 (squares) exposed to 288 L of $H_8Si_8O_{12}$. The data suggests ~6% oxygen concentration on Si(111)-7 × 7 relative to Si(100)-2 × 1.

however, no significant signal derived from an activated cluster vertex at ~2.2 eV is apparent.^{42–46} The core-level spectrum is nearly identical to the spectrum previously reported by Lee et al.⁴³ with one noticeable exception: the spectrum displayed in Figure 2 has significantly reduced intensity for the feature shifted ~1.0 eV ascribed to water contamination in the original work.

$H_8Si_8O_{12}$ reacts with ~1/3 of the dimer sites on the Si(100)-2 × 1 surface, forming a stable layer of closely packed clusters.^{42,43} Comparison of the peak area ratio of 0.104 (area of the cluster-derived feature/area of the bulk Si feature) for the data in Figure 2 to the peak area ratio of 0.762 observed for the Si $2p_{3/2}$ photoemission spectrum for Si(100)-2 × 1 exposed to a saturation dose of $H_8Si_8O_{12}$ ^{42,43} indicates a substantially lower amount of $HSiO_3$ units on the Si(111)-7 × 7 surface. Direct comparison of areas for the cluster-derived peaks (after scaling the bulk Si peaks to be equal) suggests the presence of approximately 13% cluster-derived $HSiO_3$ units on Si(111)-7 × 7 relative to Si(100)-2 × 1. Of course, differences in photoelectron attenuation resulting from structural variance may complicate this assessment given the high degree of surface sensitivity of the synchrotron core-level data obtained with a 170 eV incident photon energy (vide infra). Increased cluster adsorption on the Si(100)-2 × 1 surface leads to a greater attenuation of the bulk Si 2p core level. This means that the 13% estimate is an upper bound and the real number of $HSiO_3$ on Si(111) is likely somewhat lower, perhaps by as much as a factor of 2 as described below.

Comparison of the O 1s core-level photoemission data provides a more accurate means with which to assess surface oxide concentration following exposure of Si(111)-7 × 7 to $H_8Si_8O_{12}$. As opposed to the highly surface sensitive Si 2p core-level data obtained with exiting photoelectron kinetic energies of ~70 eV, the O 1s core-level data have been obtained with a conventional Mg K α X-ray source ($h\nu = 1253.6$ eV) yielding exiting photoelectron kinetic energies of ~720 eV. Thus, photoelectron attenuation effects are negligible for the O 1s core-level photoemission data presented in Figure 3 (Si(111)-7 × 7 (squares) and Si(100)-2 × 1 (circles); 288 L exposure of $H_8Si_8O_{12}$).

Analysis of the integrated O 1s peak areas indicates approximately 6% oxygen concentration on Si(111)-7 × 7 relative to a cluster-saturated Si(100)-2 × 1 surface. It is possible to estimate the concentration of O atoms on the cluster-exposed Si(111)-7 × 7 surface based on the ratio of the intensity of the O 1s core levels for H₈Si₈O₁₂-exposed Si(111)-7 × 7 and Si(100)-2 × 1 samples. The density of dimer sites on the Si(100)-2 × 1 surface can be determined from simple geometric arguments (3.85 Å between Si dimers within a row and 7.7 Å between dimer rows). Considering H₈Si₈O₁₂ is known to react with ~1/3 of the dimer sites on the Si(100)-2 × 1 surface and that each cluster contains precisely 12 oxygen atoms, the concentration of oxygen atoms is estimated to be ~1.3 × 10¹⁵ O atoms/cm² on Si(100)-2 × 1.⁴³ Multiplying this number by the 6% relative amount (Figure 3) generates a concentration of ~8 × 10¹³ O atoms/cm² on Si(111)-7 × 7. If one assumes a surface atom concentration of 7.8 × 10¹⁴ atoms/cm² on Si(111)-7 × 7,⁵⁷ this corresponds to ~10% oxygen concentration on the surface.

Comparison of the amount of oxide formation on Si(111)-7 × 7 as indicated by the Si 2p versus O 1s core levels is instructive. If multilayer, three-dimensional islands had formed, the relative values would be strikingly different (with the number based upon the Si 2p core level decreasing by a factor of ~2 for every effective cluster layer).^{58,59} The relative values of these two numbers (~13% cluster-derived HSiO₃ units and ~6% oxygen concentration on Si(111)-7 × 7 relative to Si(100)-2 × 1) obtained with very different incident photon energies indicates the Si-derived photoelectrons for the peak at ~3.8 eV do not have to traverse even a single extra cluster equivalent of material before escaping the surface; thus, the core-level photoemission data effectively eliminate the possibility of multilayer, three-dimensional oxide island formation on Si(111)-7 × 7.

The valence band spectrum of the interface derived from exposure of H₈Si₈O₁₂ to Si(111)-7 × 7 has also been obtained (Figure 4). Figure 4A shows the valence band spectrum as it appears in its raw data form, whereas Figure 4B shows the valence band spectrum after the spectrum of clean Si(111)-7 × 7 has been subtracted (thereby displaying only the cluster-derived signals). The bulk silicon features in the 163–165 eV region would be expected to largely disappear for this type of difference spectrum (except for intensity changes induced by differences in photoelectron attenuation), so the peak in this region is used to scale the spectra prior to subtraction. The negative feature in Figure 4B is a result of reaction of Si(111)-7 × 7 surface states present prior to H₈Si₈O₁₂ exposure. The overall shape of the valence band spectrum roughly resembles that of the spectrum of a chemisorbed layer of H₈Si₈O₁₂ on Si(100)-2 × 1 (Figure 4C); however, it appears to lack distinctive Si–H and Si–O derived features identified as arising from intact adsorbed clusters. The valence band spectrum of an unreacted, condensed layer of H₈Si₈O₁₂ on a hydrogen-terminated Si(100) surface at 133 K displays five readily discernible features corresponding to the Si–H and Si–O bonding molecular orbitals (Figure 4D).^{60,61} The absence of such features in the valence band spectrum of the thin oxide film derived from exposure

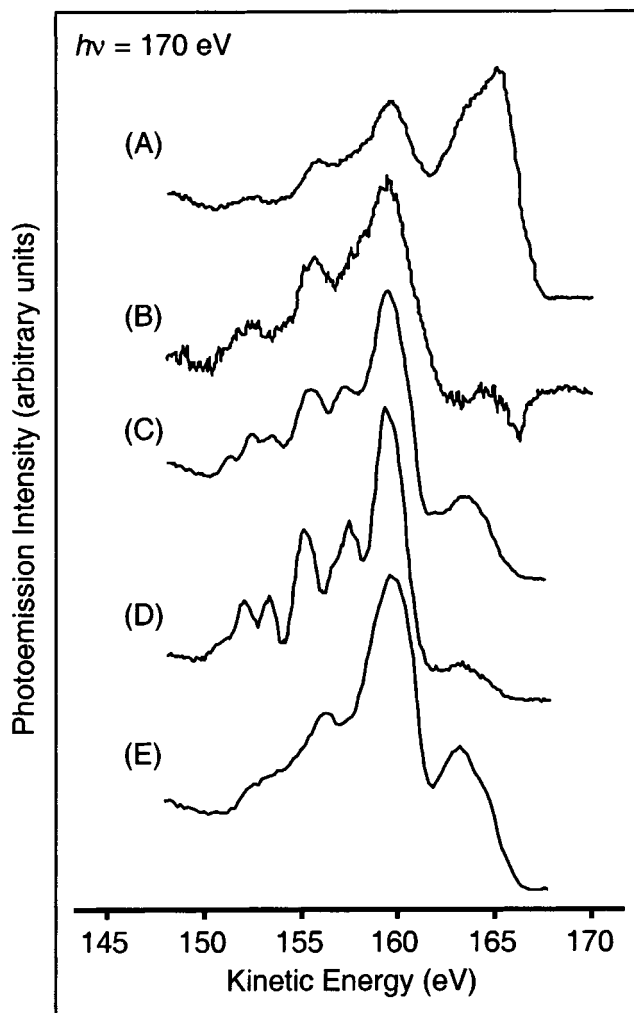


Figure 4. Valence band spectra. (A) Si(111)-7 × 7 following exposure to >1000 L of H₈Si₈O₁₂; raw data. (B) Spectrum A with spectrum of clean Si(111)-7 × 7 subtracted. (C) Si(100)-2 × 1 with chemisorbed layer of H₈Si₈O₁₂. (D) Si(100)-H with physisorbed layer of H₈Si₈O₁₂ at 133 K. (E) Hydrogenated amorphous SiO₂ formed by thermally (900 K) decomposing a monolayer of H₈Si₈O₁₂ chemisorbed to Si(100)-2 × 1. Spectra C and D have also had the spectrum of clean Si(100)-2 × 1 subtracted.

of H₈Si₈O₁₂ to Si(111)-7 × 7 suggests the cluster cages substantially decompose following reaction with the surface. Upon closer inspection, spectrum B bears a stronger resemblance to the valence band spectrum of an amorphous hydrogen-containing siloxane layer (SiOH_x) obtained by thermally decomposing a chemisorbed layer of H₈Si₈O₁₂ (via heating to 900 K) on Si(100)-2 × 1 (Figure 4E) than to a chemisorbed and/or physisorbed layer of H₈Si₈O₁₂ on Si(100)-2 × 1 (Figure 4C and 4D, respectively).^{60,61} Due to this similarity, and the absence of five identifiable features corresponding to the Si–H and Si–O bonding molecular orbitals previously obtained for chemisorbed and physisorbed layers of H₈Si₈O₁₂ on Si(100)-2 × 1, the valence band data strongly support a reaction pathway involving cluster decomposition on the Si(111)-7 × 7 surface. The signal-to-noise ratio obtained for the valence band spectrum is considerably worse than that obtained from H₈Si₈O₁₂ chemisorbed on Si(100)-2 × 1 for a similar number of scans. This is consistent with the

(57) Massoud, H. Z.; Plummer, J. D. In *The Physics and Chemistry of SiO₂ and the Si-SiO₂ Interface*; Helms, C. R., Deal, B. E., Eds.; Plenum: New York, 1988; p 251.

(58) Zhang, K. Z.; Greeley, J. N.; Banaszak Holl, M. M.; McFeely, F. R. *J. Appl. Phys.* **1997**, *82*, 2298.

(59) Zhang, K. Z.; Banaszak Holl, M. M.; McFeely, F. R. *J. Phys. Chem. B* **1998**, *102*, 3930.

(60) Zhang, K. Z.; Banaszak Holl, M. M.; McFeely, F. R. *Mater. Res. Soc. Symp. Proc.* **1997**, *446*, 241.

(61) Greeley, J. N.; Lee, S.; Banaszak Holl, M. M. *Appl. Organomet. Chem.* **1999**, *13*, 279.

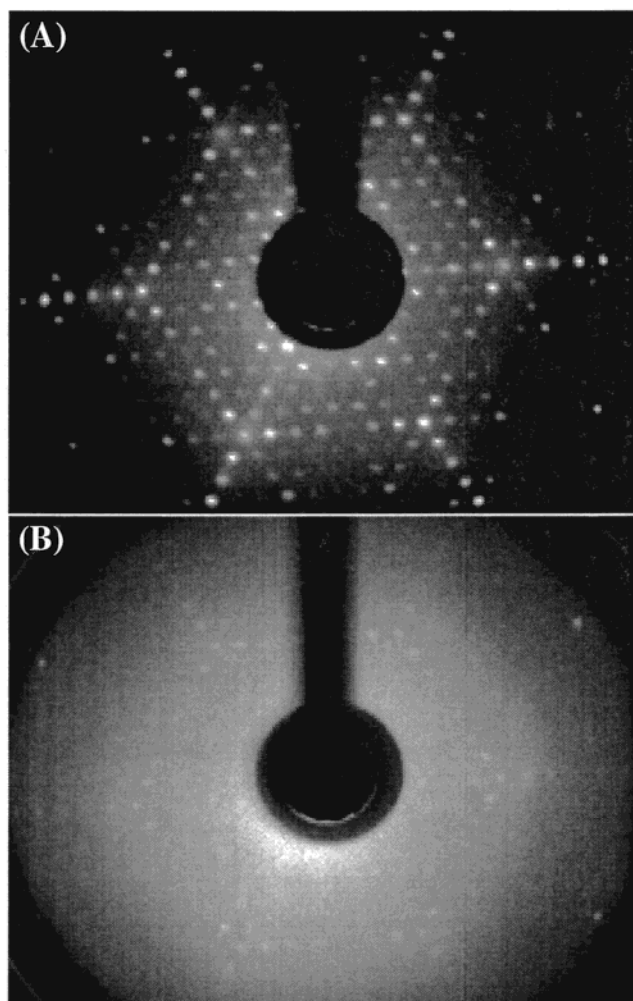


Figure 5. (A) LEED pattern of clean Si(111)-7 × 7. (B) LEED pattern of Si(111)-7 × 7 exposed to 30 L of H₈Si₈O₁₂.

lower degree of surface reactivity indicated by the Si 2p and O 1s core-level data.

In summary, the photoemission data suggest few H₈Si₈O₁₂ clusters adsorb to the Si(111)-7 × 7 surface following exposure to a saturation cluster dose. Comparison of the valence band spectra presented in Figure 4 indicates the H₈Si₈O₁₂ clusters that do adsorb to the Si(111)-7 × 7 surface undergo cage decomposition.

II. LEED Data. To study the effect of the adsorbed cluster fragments on the Si(111)-7 × 7 reconstructed surface, a LEED study has been undertaken. Figure 5A displays the LEED pattern obtained from a clean Si(111)-7 × 7 surface.^{62,63} Figure 5B presents the LEED pattern of Si(111)-7 × 7 following exposure to 30 L of H₈Si₈O₁₂. The diffraction spots of the (7 × 7) reconstruction remain clearly visible, indicating a substantial amount of clean Si(111)-7 × 7 is retained following exposure to H₈Si₈O₁₂, consistent with the low total surface oxide concentration suggested by the XPS results. A large amount of diffuse scatter is also apparent in the LEED pattern, possibly resulting from disorder introduced into clean (7 × 7) regions by the presence of adjacently bound decomposed clusters. Additionally, electron scatter by decomposed clusters present over regions of preserved (7 × 7) reconstruction may also occur. Although the reaction of

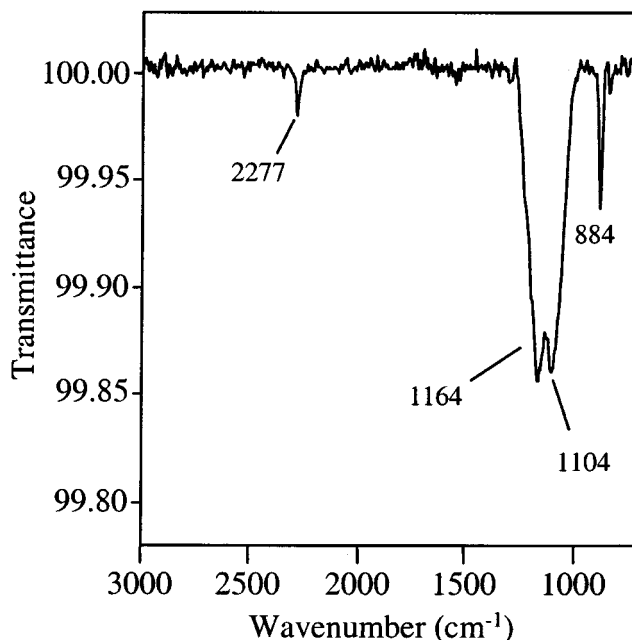


Figure 6. RAIRS (750–3000 cm⁻¹) of Si(111)-7 × 7 exposed to 700 L of H₈Si₈O₁₂. This spectrum represents 800 scans at 8 cm⁻¹ resolution ratioed to a clean Si background.

H₈Si₈O₁₂ with Si(111)-7 × 7 appears destructive to the cluster architecture, it does not appear to significantly disrupt the (7 × 7) surface reconstruction.

III. RAIRS Data. RAIRS data (750–3000 cm⁻¹) have been collected for a Si(111)-7 × 7 sample exposed to 700 L of H₈Si₈O₁₂ (Figure 6). The spectrum shows intense features at approximately 884, 1104, 1164, and 2277 cm⁻¹. The features at 884 and 2277 cm⁻¹ are assigned as cluster-derived δ(Si–H) and ν(Si–H), respectively. The large feature with splitting at 1104 and 1164 cm⁻¹ is attributed to cluster-derived ν_a(Si–O). These assignments are based on previous IR data collected for H₈Si₈O₁₂ clusters,^{64,65} H₈Si₈O₁₂ chemisorbed on Si(100)-2 × 1,^{48,52} D₈Si₈O₁₂ chemisorbed on Si(100),⁴⁸ solution data for RH₇Si₈O₁₂ clusters,⁶⁶ and density functional theory calculations for H₈Si₈O₁₂ chemisorption to a model Si(100) surface dimer.^{52,53}

When compared to the RAIRS spectrum of a chemisorbed layer of closely packed H₈Si₈O₁₂ clusters on Si(100)-2 × 1 (Figure 7C), the RAIRS spectrum of Si(111)-7 × 7 exposed to 700 L of H₈Si₈O₁₂ (Figure 7A) contains noticeable differences. Figure 7C displays intense features at 888, 1179, and 2271 cm⁻¹ assigned as δ(Si–H), ν_a(Si–O), and ν(Si–H), respectively. The details and full explanation for these assignments are described elsewhere.^{48,52,53} The spectrum of monodispersed (i.e., not closely packed) H₈Si₈O₁₂ clusters chemisorbed to Si(100)-2 × 1 (0.25 L H₈Si₈O₁₂ exposure) displays intense features at 884, 1157, 1078, and 2271 cm⁻¹ (Figure 7B). The features at 884 and 2277 cm⁻¹ are assigned as δ(Si–H) and ν(Si–H), respectively. The large feature with splitting at 1157 and 1078 cm⁻¹ is attributed to ν_a(Si–O). Note that the ν_a(Si–O) frequency for monodispersed clusters on Si(100)-2 × 1 (1157 and 1078 cm⁻¹; Figure 7B) is considerably lower than is observed for a chemisorbed layer of closely

(64) Bärtsch, M.; Bornhauser, P.; Calzaferri, G.; Imhof, R. *J. Phys. Chem.* **1994**, *98*, 2817.

(65) Calzaferri, G.; Imhof, R.; Tornroos, K. W. *J. Chem. Soc., Dalton Trans.* **1994**, 3123.

(66) Marcolli, C.; Calzaferri, G. *Appl. Organomet. Chem.* **1999**, *13*, 213.

(62) Schlier, R. E.; Farnsworth, H. E. *J. Chem. Phys.* **1959**, *30*, 917.

(63) Tong, S. Y.; Huang, H.; Wei, C. M.; Packard, W. E.; Men, F. K.; Glander, G.; Webb, M. B. *J. Vac. Sci. Technol., A* **1988**, *6*, 615.

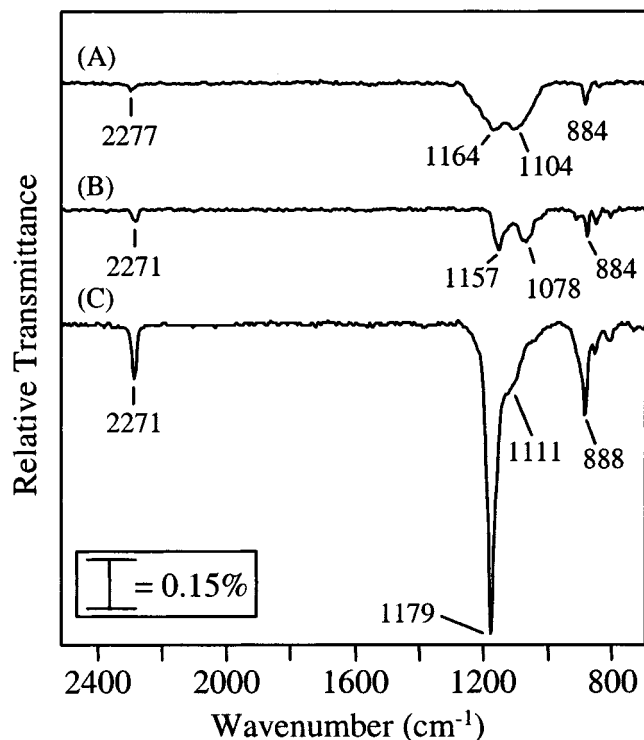


Figure 7. (A) RAIRS (750–2500 cm^{-1}) of Si(111)-7 \times 7 exposed to 700 L of $\text{H}_8\text{Si}_8\text{O}_{12}$. (B) RAIRS of a submonolayer of $\text{H}_8\text{Si}_8\text{O}_{12}$ chemisorbed to Si(100)-2 \times 1 resulting from exposure of 0.25 L of $\text{H}_8\text{Si}_8\text{O}_{12}$ to a clean Si(100)-2 \times 1 sample. (C) RAIRS (750–2500 cm^{-1}) of a monolayer of $\text{H}_8\text{Si}_8\text{O}_{12}$ chemisorbed to Si(100)-2 \times 1. Each spectrum represents (A) 800 and (B, C) 256 scans at 8 cm^{-1} resolution ratioed to a clean Si background.

packed clusters on Si(100)-2 \times 1 (1179 and 1111 cm^{-1} ; Figure 7C). The cluster concentration/proximity dependency of the $\nu_a(\text{Si}-\text{O})$ frequency shift has been previously observed for $\text{H}_8\text{Si}_8\text{O}_{12}$ chemisorbed to Au(111) and primarily attributed to anomalous dispersion and vibrational coupling.^{67,68} From the data presented in Figure 7B and Figure 7C, it is apparent that similar frequency shifts are observed for increasing $\text{H}_8\text{Si}_8\text{O}_{12}$ exposure to Si(100)-2 \times 1. Interestingly, the $\nu_a(\text{Si}-\text{O})$ frequency for $\text{H}_8\text{Si}_8\text{O}_{12}$ -derived fragments on Si(111)-7 \times 7 (1164 and 1104 cm^{-1} ; Figure 7A) is also considerably lower than the $\nu_a(\text{Si}-\text{O})$ frequency observed for a chemisorbed layer of closely packed clusters on Si(100)-2 \times 1 (1179 and 1111 cm^{-1} ; Figure 7C), but is slightly higher than the $\nu_a(\text{Si}-\text{O})$ frequency observed for monodispersed clusters on Si(100)-2 \times 1 (1157 and 1078 cm^{-1} ; Figure 7B). The $\nu_a(\text{Si}-\text{O})$ frequency shift observed for $\text{H}_8\text{Si}_8\text{O}_{12}$ -derived fragments on Si(111)-7 \times 7 suggests that oxide is present on the surface in the form of intermittent two-dimensional islands.

Comparison of the $\nu_a(\text{Si}-\text{O})$ and $\nu(\text{Si}-\text{H})$ regions yields some basic information concerning reactivity differences of $\text{H}_8\text{Si}_8\text{O}_{12}$ with Si(111)-7 \times 7 and Si(100)-2 \times 1. Most noticeably, the $\nu_a(\text{Si}-\text{O})$ peak is much less intense for the Si(111)-7 \times 7 sample than for the Si(100)-2 \times 1 sample, suggesting a lower amount of cluster-derived oxide on Si(111)-7 \times 7 than is observed for Si(100)-2 \times 1, in good agreement with the XPS data. The $\nu_a(\text{Si}-\text{O})$ peak is also much broader and displays a characteristic splitting for the Si(111)-7 \times 7 sample unseen in the spectrum for a

chemisorbed layer of $\text{H}_8\text{Si}_8\text{O}_{12}$ on Si(100)-2 \times 1. Additionally, the relative intensities of the $\nu_a(\text{Si}-\text{O})$ and $\nu(\text{Si}-\text{H})$ regions are strikingly different. The $\nu(\text{Si}-\text{H})/\nu_a(\text{Si}-\text{O})$ ratio for the Si(111)-7 \times 7 sample exposed to a saturation dose of $\text{H}_8\text{Si}_8\text{O}_{12}$ (Figure 7A) is ~ 0.03 , whereas the ratio for a chemisorbed layer of closely packed clusters on Si(100)-2 \times 1 (Figure 7C) is ~ 0.06 . A variety of factors can affect the observed intensities in RAIRS spectra; however, low coverages of intact $\text{H}_8\text{Si}_8\text{O}_{12}$ clusters chemisorbed to Si(100)-2 \times 1 (Figure 7B) share many features similar to Figure 7A and give a $\nu(\text{Si}-\text{H})/\nu_a(\text{Si}-\text{O})$ ratio of ~ 0.07 . Although the comparison of the $\nu(\text{Si}-\text{H})/\nu_a(\text{Si}-\text{O})$ ratios is not conclusive, it does suggest the $\text{H}_8\text{Si}_8\text{O}_{12}$ clusters have decomposed on Si(111)-7 \times 7, losing some Si-H bonds in the process. This is consistent with the valence band spectra (Figure 4A,B), which also suggest cluster decomposition, and compare well with thermally degraded clusters on Si(100)-2 \times 1 having a decreased Si-H bond content (Figure 4E).

The combined XPS and RAIRS data support the decomposition of clusters resulting in isolated regions of hydrogenated silicon oxide upon exposure of Si(111)-7 \times 7 to a saturating dose of $\text{H}_8\text{Si}_8\text{O}_{12}$; however, these spectroscopic techniques do not provide information on the spatial arrangement and size of the hydrogenated oxide regions. To gain a better understanding of the structure of these regions relative to the Si(111)-7 \times 7 substrate, a STM study has been initiated.

IV. STM Data. The Takayanagi et al. dimer-atom-stacking fault (DAS) model is the generally agreed upon model for the (7 \times 7) reconstructed Si(111) surface.⁶⁹ In the DAS model, there are an equal number (six apiece) of “corner adatoms” (atoms adjacent to a “corner hole”) and “center adatoms” (atoms not adjacent to a “corner hole”) in a unit cell with the “rest atom” layer ~ 4 Å below the adatom layer. Each center adatom has two nearest-neighbor rest atoms. Each corner adatom has only one nearest-neighbor rest atom. Both adatoms and rest atoms occupy tetrahedral positions and have one dangling bond (free electron). Because the adatoms are located atop the rest atom layer and have an electron density with energy at or near the Fermi level (E_F), the surface adatoms are most prominently imaged by STM.^{69–72}

A large-scale 1000 Å \times 1000 Å filled states constant-current topograph of a Si(111)-7 \times 7 surface following exposure to 12 L of gaseous $\text{H}_8\text{Si}_8\text{O}_{12}$ is displayed in Figure 8A (sample bias, $V_s = -1.52$ V; tunneling current, $I_T = 2.31$ nA). Atomic resolution of the Si(111)-7 \times 7 sample surface is apparent, clearly showing the preservation of the (7 \times 7) surface reconstruction following exposure to $\text{H}_8\text{Si}_8\text{O}_{12}$, in good agreement with the LEED data. Additionally, the surface appears mottled with numerous bright protrusions and dark atomic “vacancies”. Figure 8B is a height-mapped surface rendering of the boxed region in Figure 8A displaying the surface protrusions, as they appear to occupy one to several substrate lattice sites. The surface protrusions in Figure 8A have a range of apparent heights from approximately 0.5 to 2.5 Å, with the majority of features ~ 2 Å in apparent height, and vary in width from ~ 5 to 15 Å. Figure 8C shows the horizontal cross-sectional profiles from the corresponding numbered surface features in Figure 8A. The apparent

(69) Takayanagi, K.; Tanishiro, Y.; Takahashi, M.; Takahashi, S. *J. Vac. Sci. Technol., A* **1985**, *3*, 1502.

(70) Binnig, G.; Rohrer, H.; Gerber, C.; Weibel, E. *Phys. Rev. Lett.* **1983**, *50*, 120.

(71) Tromp, R. M.; Hamers, R. J.; Demuth, J. E. *Phys. Rev. B* **1986**, *34*, 1388.

(72) Tersoff, J.; Hamann, D. R. *Phys. Rev. B* **1985**, *31*, 805.

(67) Nicholson, K. T.; Zhang, K. Z.; Banaszak Holl, M. M.; McFeely, F. R.; Pernisz, U. C. *Langmuir* **2000**, *16*, 8396.

(68) Nicholson, K. T.; Zhang, K. Z.; Banaszak Holl, M. M.; McFeely, F. R.; Calzaferrri, G.; Pernisz, U. C. *Langmuir* **2001**, *17*, 7879.

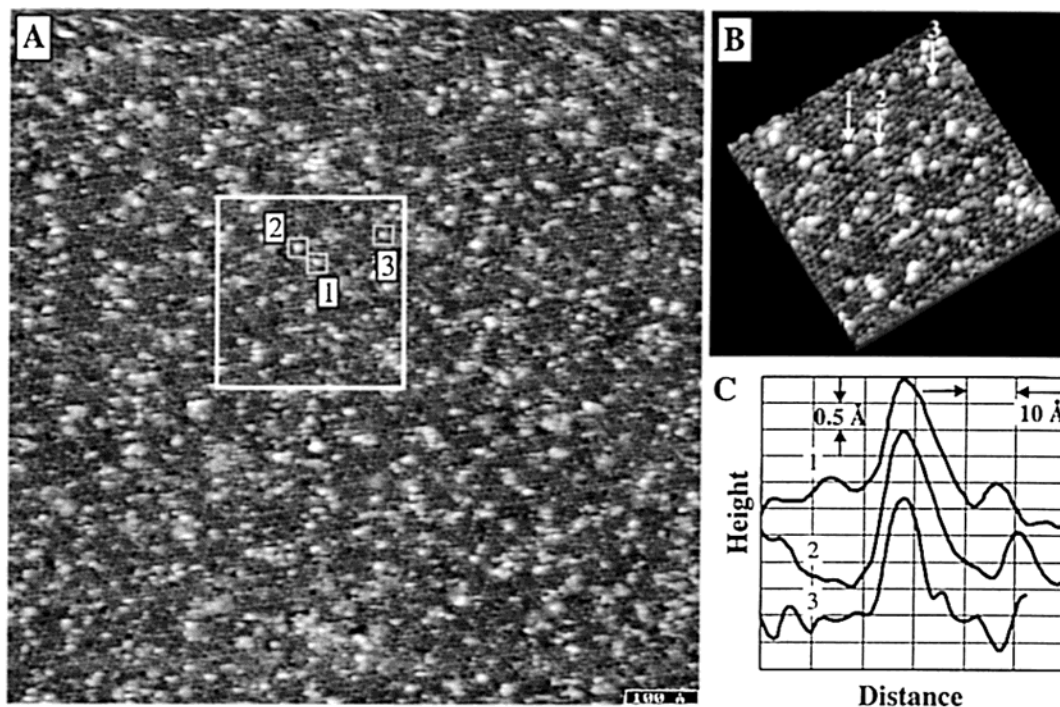


Figure 8. Constant-current UHV STM topographs of Si(111)-7 × 7 exposed to 12 L of $\text{H}_8\text{Si}_8\text{O}_{12}$. (A) 1000 Å × 1000 Å region; $V_s = -1.52$ V, $I_T = 2.31$ nA. (B) Height-mapped surface rendering from the boxed region in part A displaying the cluster-derived surface features relative to the surface adatoms. (C) Horizontal cross-sectional profiles from the corresponding surface features in part A. Profiles show an apparent feature width of ~5–15 Å and height of ~2 Å.

heights and widths of the features in Figure 8 differ dramatically from those observed for individual intact clusters chemisorbed on Si(100)-2 × 1 (which appear as ordered, regular arrangements of four distinct dots oriented in a square having an apparent height of ~0.8 Å and apparent width of ~5–6 Å, respectively).⁴⁹

Higher resolution images of Si(111)-7 × 7 exposed to $\text{H}_8\text{Si}_8\text{O}_{12}$ clearly show the surface protrusions in relation to the underlying substrate atoms. Figure 9A displays a 400 Å × 400 Å filled states image of a Si(111)-7 × 7 sample exposed to 360 L of $\text{H}_8\text{Si}_8\text{O}_{12}$ ($V_s = -2.03$ V; $I_T = 0.55$ nA). Plotted in Figure 9B is a normalized height histogram of the image presented in Figure 9A. Height histograms plot STM topographs as a function of image pixel frequency versus pixel height. Through analysis of height histograms of the Si(111)-7 × 7/ $\text{H}_8\text{Si}_8\text{O}_{12}$ images, it is possible to estimate the areal extent the surface protrusions occupy per image region. Because the images contain high dispersions of protrusions per image area, a greater fraction of image pixels lie on or near protrusion edges, thus causing an overlapping of peaks in the height histograms and resulting in an overall curve with an asymmetric tailing to the positive pixel height side. However, curve fits of the height histograms allow facile extraction of the total area occupied by surface features relative to the substrate via comparison of integrated curve fit peak areas. Numerous height histograms were curve fit in this manner to derive a total protrusion area of 23% ± 5% relative to the Si(111)-7 × 7 surface. Because STM provides data on an individual atomic level, a degree of variation in total surface feature area from region to region is to be expected.

Statistical analysis of this image and several others reveals little preference for protrusion sites to particular regions of the Si(111)-7 × 7 unit cell. Atom counting statistics yield a near 1:1 ratio of “missing” corner and center adatoms from image to image. Additionally, there is an approximate 1:1 ratio of apparently unreacted corner

and center adatoms. No preference for adsorption to faulted or unfaulted halves of the Si(111)-7 × 7 unit cell is apparent. Similar atom counting statistical procedures have been employed to determine preferential surface sites of adsorbates on Si(111)-7 × 7;⁷³ however, Figures 8 and 9 indicate that the reaction of $\text{H}_8\text{Si}_8\text{O}_{12}$ with Si(111)-7 × 7 produces surface features independent of specific surface lattice sites.

Unlike the chemisorption of $\text{H}_8\text{Si}_8\text{O}_{12}$ to Si(100)-2 × 1 (in which internal resolution of the electronic states of individual, intact clusters is readily apparent in filled states STM images),⁴⁹ STM images of Si(111)-7 × 7 dosed with $\text{H}_8\text{Si}_8\text{O}_{12}$ suggest cluster decomposition occurs following exposure to the surface. The dramatically increased apparent heights of cluster-derived features observed by STM are likely the result of dangling bonds associated with decomposed clusters and/or the density of states associated with adsorbed cluster fragments. Recall this is consistent with the information gained from comparing silicon oxide surface concentration estimates obtained from Si 2p core levels to those obtained from O 1s core-level photoemission data, the results of which eliminate the possibility of multilayer island formation. The variation in apparent widths of the surface protrusions in the STM data could result from adjacent or adjoining decomposed clusters or cluster fragments, suggested from the RAIRS data.

STM images of oxidized and partially oxidized Si(111)-7 × 7 surfaces share many characteristics similar to the features observed in Figures 8 and 9.^{19,24–26,74} Assignments of the features observed in oxidized and partially oxidized Si(111)-7 × 7 STM images include oxygen insertion into one or multiple Si back-bonds, an oxygen atom bonded atop a single surface adatom, and adsorption of molecular O_2 atop surface adatoms; however, all of these assignments

(73) Avouris, P. *J. Phys. Chem.* **1990**, *94*, 2246.

(74) Dujardin, G.; Mayne, A.; Comtet, G.; Hellner, L.; Jamet, M.; Le Goff, E.; Millet, P. *Phys. Rev. Lett.* **1996**, *76*, 3782.

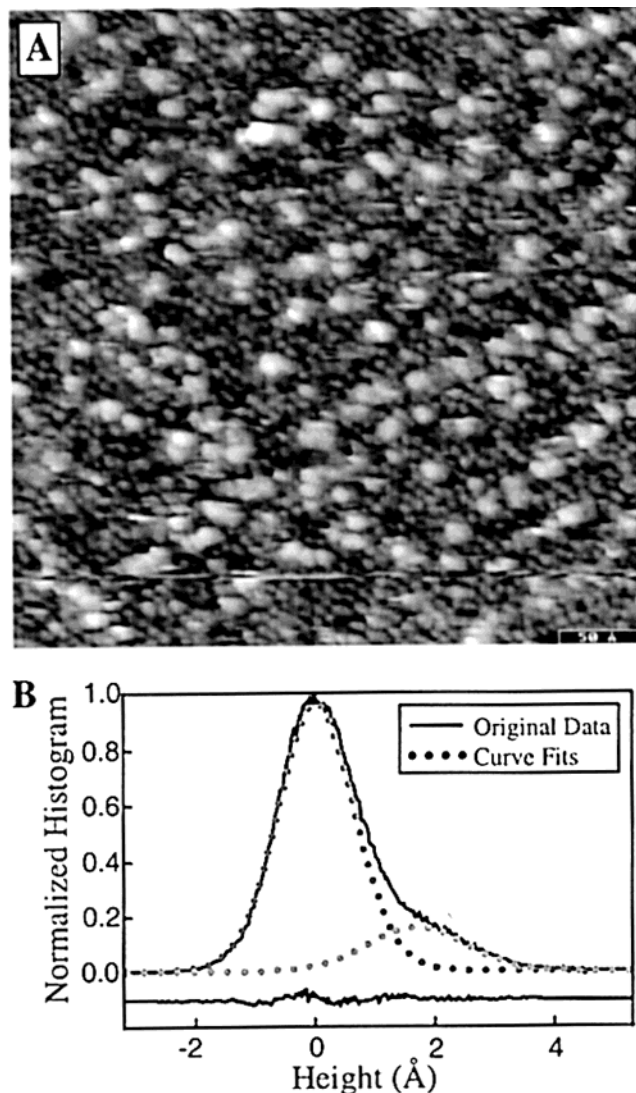


Figure 9. (A) Constant-current $400 \text{ \AA} \times 400 \text{ \AA}$ filled states image of Si(111)- 7×7 exposed to 360 L of $\text{H}_8\text{Si}_8\text{O}_{12}$; $V_s = -2.03 \text{ V}$, $I_T = 0.55 \text{ nA}$. (B) Normalized height histogram plot of image A. The height histogram indicates a total protrusion area of $23\% \pm 5\%$ relative to the Si(111)- 7×7 substrate.

are debated in the literature and a definitive structure for these ultrathin oxide films remains elusive. Recall that the only apparent cluster-derived signal in the XPS Si $2p_{3/2}$ core-level spectrum of Si(111)- 7×7 exposed to $\text{H}_8\text{Si}_8\text{O}_{12}$ (Figure 2) can be attributed to HSiO_3 or SiO_4 fragments, and the RAIRS spectra suggest both are likely. Due to the similarity of Figures 8 and 9 to STM images of oxidized and partially oxidized Si(111)- 7×7 surfaces, it could be speculated that the reaction of $\text{H}_8\text{Si}_8\text{O}_{12}$ with Si(111)- 7×7 may also result in oxygen insertion into Si back-bonds, adsorption of cluster fragments atop Si adatoms, or some combination of both. However, since no appreciable intensity is present in the Si $2p$ core-level photoemission data in the region between ~ 1 and 2 eV where oxygen insertion species should appear, adsorption of HSiO_3 cluster fragments via the formation of Si–O bonds to the surface is the more likely scenario. The high dispersion of cluster fragments apparent in the STM images is in good agreement with the formation of a discontinuous ultrathin oxide film inferred from the XPS and RAIRS data. Furthermore, the increased apparent widths of cluster-derived features on Si(111)- 7×7 , relative to those observed for individual chemisorbed, intact

clusters on Si(100)- 2×1 ,⁴⁹ are suggestive of two-dimensional islanding of adsorbed cluster fragments on the surface, in good agreement with the RAIRS data.

Considering that the STM images contain both surface protrusions and atomic “vacancies” complicates definitive interpretation of the STM height histogram data. Analysis of the STM height histogram data may lead one to incorrectly assume that reacted Si(111)- 7×7 surface sites are necessarily imaged *only* as surface protrusions. Previous STM studies of oxidized and partially oxidized Si(111)- 7×7 surfaces suggest oxidized regions may appear as both bright protrusions and dark atomic “vacancies”.^{19,24–26,74} However, dangling bonds of decomposed clusters and/or the density of states associated with adsorbed cluster fragments are likely to have a positive contrast contribution in the STM images. The most definitive structural information gleaned from the STM data supports $\text{H}_8\text{Si}_8\text{O}_{12}$ cluster decomposition resulting in a random distribution of two-dimensional oxide islands comprised of cluster fragments on the Si(111)- 7×7 surface.

Recent theoretical studies have suggested $\text{H}_8\text{Si}_8\text{O}_{12}$ clusters partially decompose on Si(100)- 2×1 via Si–O–Si bond scission along a cluster edge;^{75,76} however, the proposed “cracked cluster” bonding geometry is ruled out by STM studies.⁴⁹ In the studies presented here for Si(111)- 7×7 , the spectroscopic effects of cluster decomposition are clearly observed by multiple experimental methods. In this instance, $\text{H}_8\text{Si}_8\text{O}_{12}$ cluster decomposition results in the following: (1) the loss of distinct features associated with an activated Si cluster vertex and surface Si atom in the Si $2p_{3/2}$ core-level XPS spectrum, (2) the loss of distinct valence band features deriving from an intact $\text{H}_8\text{Si}_8\text{O}_{12}$ cluster observed by synchrotron radiation photoemission measurements, (3) a substantially smaller amount of observable Si–H as indicated by the $\nu(\text{Si–H})/\nu_a(\text{Si–O})$ ratio in RAIRS spectra, and (4) a dramatic increase in apparent height and loss of features associated with the electronic states of an adsorbed intact cluster as observed in STM images.

Summary and Conclusions

XPS, LEED, RAIRS, and STM have been used to characterize the structure of the discontinuous ultrathin oxide film formed as a result of exposing gaseous $\text{H}_8\text{Si}_8\text{O}_{12}$ hydrosilanesquioxane clusters to Si(111)- 7×7 . Analysis of data collected from all four techniques indicates a small number of the clusters adsorb to the Si(111)- 7×7 surface, resulting in a random distribution of two-dimensional hydrogenated oxide islands comprised of decomposed clusters and/or cluster fragments. This is in stark contrast to the formation of a saturated chemisorbed layer of intact clusters observed for the reaction of $\text{H}_8\text{Si}_8\text{O}_{12}$ with Si(100)- 2×1 .^{42–49,52,77}

The preservation of the hydrosilanesquioxane cluster cage following reaction with the silicon surface may be dependent upon the proximity of reactive surface sites. The Si(100)- 2×1 surface contains Si dimers separated by 3.85 \AA within a row, with Si dimer atom pairs 2.35 \AA apart. Nearest-neighbor Si atoms of the Si(111)- 7×7 surface (an adatom and rest atom) are separated by approximately 4 \AA . Furthermore, the adatom layer is physically stacked atop the rest atom layer. The larger

(75) Raghavachari, K.; Eng, J. J. *Phys. Rev. Lett.* **2000**, *84*, 935.

(76) Raghavachari, K.; Pasquarello, A.; Eng, J. J.; Hybertson, M. S. *Appl. Phys. Lett.* **2000**, *76*, 3873.

(77) McFeely, F. R.; Zhang, K. Z.; Banaszak Holl, M. M.; Lee, S.; Bender, J. E., IV. *J. Vac. Sci. Technol., B* **1996**, *14*, 2824.

separation distance between nearest-neighbor reactive sites on Si(111)-7 × 7 relative to Si(100)-2 × 1 may inhibit a Si-H bond activation from occurring. Additionally, because the rest atoms lie in the second layer relative to the adatom layer, steric hindrance may prohibit an Si-H bond activation of H₈Si₈O₁₂ at these sites on the Si(111)-7 × 7 surface.

Acknowledgment. Dow-Corning Corporation, RHK Technology, Inc., and the NSF (DMR-0093641 and DMR-9802586) are gratefully acknowledged for support of this work. Mehmet Dokmeci is thanked for cutting the silicon samples used for the RAIRS experiments. Phil Holland

is thanked for computer programming used in the analysis of STM topograph height histogram data. M.M.B.H. is grateful for an Alfred P. Sloan Research Fellowship (1999-2002). K.S.S. and B.J.L. thank the NSF for IGERT fellowships (DGE-9972776). Portions of this work were carried out at the National Synchrotron Light Source, Brookhaven National Laboratory, which is supported by the U.S. Department of Energy (Division of Materials Science and Division of Chemical Sciences of the Office of Basic Energy Sciences) under Contract No. DE-AC02-98CH10886.

LA025615J